RSC Advances

One pot synthesis of Fe3O4/MnO2 core/shell structured nanocomposites and their application for microwave absorbers

Journal:	*RSC Advances*
Manuscript ID:	RA-ART-11-2014-014753.R2
Article Type:	Paper
Date Submitted by the Author:	17-Feb-2015

Complete List of Authors:	Liu, Xianguo; Institute of Metal Research, Shenyang National Laboratory for Material Science Wu, Niandu; Anhui University of Technology, School of Materials Science and Engineering Cui, Caiyun; Anhui University of Technology, School of Materials Science and Engineering Bi, Nannan; School of Materials Science and Engineering, Anhui University of technology Sun, Yuping; Center for Engineering practice and Innovation Education, Anhui University of technology

Cite this: DOI: 10.1039/c0xx00000x

www.rsc.org/advances

PAPER

One pot synthesis of Fe_3O_4/MnO_2 core/shell structured nanocomposites and their application for microwave absorbers

Xianguo Liu,*[a] Niandu Wu,[a] Caiyun Cui,[a] Nannan Bi,[a] and Yuping Sun[b]

Received (in XXX, XXX) Xth XXXXXXXXX 20XX, Accepted Xth XXXXXXXXX 20XX

DOI: 10.1039/b000000x

Fe_3O_4/MnO_2 core/shell structured nanocomposites have been synthesized by a one-pot approach at ambient temperature and pressure. The morphologies of the prepared Fe_3O_4/MnO_2 nanoparticles were governed by the molar ratio of Mn/Fe in the precursor. When the molar ratio of Mn/Fe is 1:10, the nanocomposites exhibit the special microstructure, in which MnO_2 nanrods are formed on the surface of spherical Fe_3O_4 nanoparticles. With the increase of Mn/Fe ratio to 1:2, the core-shell structured nanoparticles with Fe_3O_4 nanoparticles as cores and MnO_2 as shells are obtained. Microwave absorption properties of core-shell Fe_3O_4/MnO_2 nanocomposites were studied in the 2-18 GHz frequency range. The microwave absorption performance of Fe_3O_4/MnO_2 nanocomposites exhibited the remarkable enhancements compared with the pure Fe_3O_4 nanoparticles, ascribed to the fact that MnO_2 nanostructures can improve the dielectric loss factor and the EM matching degree. The absorption peaks of the Fe_3O_4/MnO_2-paraffin composites have a red shift compared with those of the Fe_3O_4-paraffin composites. Due to the MnO_2 nanorods on the surface of Fe_3O_4 nanoparticles, the produced microcurrent can reduce the electron transition energy and lead to the better microwave absorption in the Fe_3O_4 nanoparticles/MnO_2 nanorods nanocomposites.

1. Introduction

Serious electromagnetic (EM) interference problems arising from the rapidly expanding communication devices, such as wireless internet, mobile telephones and military application have sparked a priority towards research on EM wave loss materials. The EM wave loss materials can absorb energy from EM wave and convert the EM energy to the thermal through the combined action of dielectric loss and magnetic loss.[1-5] For application, it is desirable to achieve strong EM wave absorption (99% absorption) in the whole 2-18 GHz range for a thin absorber layer with low mass density. The EM wave loss performance can be determined by the complex permeability/permittivity, EM impedance matching and the microstructure of the absorbents.[2] Many efforts have been paid on fabricating various microwave absorption materials. Nanocomposites consisting of magnetic metals and dielectric materials have attracted extensive interests in microwave absorption in the 2-18 GHz range.[6-10]

For certain severe working environment in aerospace industry or devices for high-temperature applications, development of EM wave materials with strong anti-oxidation abilities is needed. At this point, both metals and carbon-based materials could be oxidized when applied to high-temperature working environment, resulting in the degradation of EM absorption performance. To develop EM wave absorption materials for high-temperature applications, thermal stability is highly required. Basic EM absorption mechanisms suggest that good absorbers should have mobile charge carriers for absorption.[11, 12] At this point, charge carriers in semiconductor could be excited at elevated temperature, leading to the increase in charge carriers at higher temperature. Therefore, semiconductor oxides seem to be candidates for EM wave absorber at high temperature.

As typical semiconductor oxides, MnO_2 is an attractive kind of dielectric absorption materials with broad frequency bandwidth and its wave attenuation property can be attributed mainly to its high dielectric constant. Meanwhile, MnO_2 also possesses the advantage of its cheap, natural abundance and environmental friendliness.[13] So far, numerous studies on the EM properties of MnO_2 materials have been reported, including nanowires, nanorods, microspheres, and hierarchical structures.[14-17] MnO_2 urchin-like nanostructures exhibited good microwave absorption performances in the frequency range of 2-18 GHz.[16] Duan and Guan et al. studied the dielectric and EM characteristics of MnO_2 materials with different crystalline and morphological structures prepared through different methods.[13,16] Due to its superior property of large magnetic loss and great resistivity, Fe_3O_4-based nanocomposites have been widely prepared and their EM absorption performances have been deeply investigated.[18-20] However, the EM absorption performances of Fe_3O_4/MnO_2 nanocomposites have been rarely studied.

In this work, a series of Fe_3O_4/MnO_2 nanocomposites were synthesized at 90 ^oC by a facile and green one pot hydrothermal method through the adjustment of the molar ratio of Mn/Fe (0:10, 1:10, and 1:2). The inexpensive $FeSO_4$ and $KMnO_4$ were applied as precursors of Fe and Mn, respectively. Moreover, the morphology can be controlled through the adjustment of the molar ratio of Mn/Fe. The morphology, microstructure, and

microwave absorption properties of these nanocomposites have been investigated systematically and the effects of the MnO_2 component are discussed.

2. Experimental

2.1 Synthesis of Fe_3O_4/MnO_2 nanocomposites

Hydrothermal method was used to fabricate the core/shell structured nanocapsules with initial Mn/Fe molar ratios of 0:10 (sample 1), 1:10 (sample 2) and 1:2 (sample 3) at 90°C with continuous gentle stirring. $FeSO_4•7H_2O$ (2.5 mmol) were dissolved in 100 mL deionized water and kept for 1h. And then, 1 mL of 5.0 M NaOH was added into the solution, generating a green suspension. Subsequent, an aqueous solution of $KMnO_4$ was added into the reaction solution dropwise, producing the dark brown precipitate. After aging the dark brown precipitate for 12 h, the Fe_3O_4/MnO_2 nanocomposites are finally obtained thoroughly washed with deionized water and ethanol alternately, followed by drying in a vacuum drying oven at 60 °C.

2.2 Materials characterizations

The phase, morphology and microstructure of the products were characterized by X-ray diffraction (XRD, Brucker D8 Advance diffractometer), scanning electron microscopy (SEM, JEOL-6300F) equipped with energy dispersive spectrometer (EDS, Oxford, UK) and high-resolution transmission electron microscopy (HRTEM, JEOL-2010F) at an acceleration voltage of 200 kV, respectively.

2.3 Electromagnetic absorbing measurement

The details on the preparation for EM measurement samples were described elsewhere.[2-4] The mass ratio of the products in the paraffin-bonding composites was set to be 40 wt%. The complex permittivity (ε_r) and the complex permeability (μ_r) of the composites were obtained in a frequency (f) range of 2 to 18 GHz using an Agilent 8722ES network analyzer. The ε_r and μ_r were calcuated from the S-parameters tested by the calibrated vector network analyzer, using a simulation program with the Reflection/Transmission Nicolson-Ross model.

3. Results and Discussion

Fig.1 shows the XRD patterns of three as-synthesized samples. For three samples, the XRD patterns show that the reflections of (111), (220), (311), (222), (400), (422), (511), (440), (620), (533) and (444) can be readily indexed to magnetite Fe_3O_4 [JCPDS Card No: 19-0629] with a space group of *Fd-3m*. No peaks of MnO_2 in sample 2 are observed due to their small amount and breaking down of the periodic boundary condition on the surface of Fe_3O_4 nanoparticles.[21] An amorphous peak located at 21.4° in sample 3 indicates the existence of amorphous MnO_2. The MnO_2 structure in sample 2 and sample 3 will be further confirmed in the HRTEM analysis in the paper.

As shown in Figs. 2(a)-(c), the typical morphologies of the three samples are examined using SEM. For sample 1(Fig. 2(a)), it can be seen that the bare spheres with smooth surface have an averaged size of about 40 nm. After the $KMnO_4$ (Mn/Fe molar ratios of 1:10) was added (sample 2), some nanorods with the length of about 15 nm and diameter of about 5 nm were observed to form and anchor on the surface of the nanosphere with an averaged size of 40 nm (Fig.2(b)). With the increase of Mn/Fe molar ratios to 1:2(sample 3), the products exhibit the sphere shape with an averaged sized of 60 nm (Fig.2(c)), which is larger than that of sample 1. In order to discriminate between sample 1 and sample 3, EDS spectra (Fig.2(d)) is used to further evidence the element component. It is seen clearly that the Mn element exists in sample 3, which is in good agreement with the XRD results. The detailed microstructure of these three samples is further investigated by HRTEM. It is obvious that no 'core/shell' type microstructure of nanoparticles in sample 1 can be observed in the HRTEM image of Fig.3 (a). The lattice plane spacing of the nanoparticles is about 0.253 nm, which corresponds to the (311) planes of Fe_3O_4. Fig.3 (b) demonstrates the typical HRTEM image of sample 2. A single nanorod is clearly seen on the surface of Fe_3O_4 nanoparticle. As shown in the inset of Fig.3(b), the measured interplanar distance of 0.41 nm in the nanorod can be assigned to the characteristic interplanar distance of (131) of MnO_2. The HRTEM image in Fig.3(c) reveals the nanocomposites in sample 3 own a core/shell-type structure consisting of an inner Fe_3O_4 nanoparticle core encapsulated by an amorphous shell with thickness of about 10 nm. The amorphous shell should be MnO_2 on basis of the XRD, the EDS results and the experiment process. Except the MnO_2 shell, the size of Fe_3O_4 nanoparticles core in sample 3 is equal to that of sample 1.

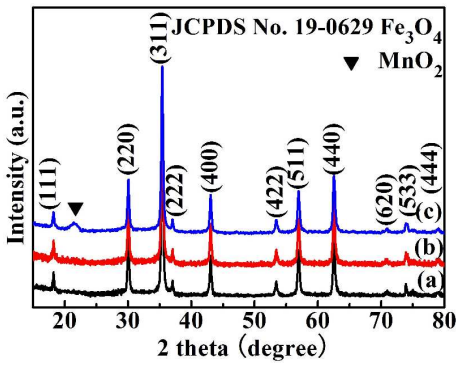

Fig.1 XRD patterns of (a) sample 1, (b) sample 2 and (c) sample 3.

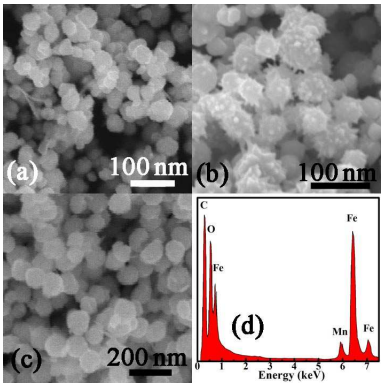

Fig.2 SEM images of (a) sample 1, (b) sample 2 and (c) sample 3. (d) EDS spectra of sample 3.

On the basis of above experimental results and the literature, the synthesis process of the Fe_3O_4/MnO_2 nancomposites is proposed, as schemed in Fig.4. For three samples, the mechanism of formation of green $Fe(OH)_2$ follows the Eq. (1). For the synthesis of sample 1, the $Fe(OH)_2$ were oxidized by oxygen dissolved in the solution to ferric hydroxide (Eq.(2)), and the formation of Fe_3O_4 nanoparticles was achieved through a dehydration reaction of ferrous hydroxide and ferric hydroxide (Eq.(3)).[22] For the sample 2 and sample 3, the redox reactions between $Fe(OH)_2$ and $KMnO_4$ took place rapidly with the formation of dark sediments once $KMnO_4$ was added into the green $Fe(OH)_2$ suspension (Eq.(4)).[22] Fe_3O_4 is a well-known ferrimagnetic oxide. MnO_2 is one kind of diluted magnetic semiconductors. At the initial stage of the sample 2 with the Mn/Fe ratio of 1:10, the generated MnO_2 nanoparticles are randomly adhered onto the surface of the Fe_3O_4 nanoparticles, due to the isotropic magnetic field of spherical Fe_3O_4 nanoparticles. Afterward, the distribution of magnetic field is changed. Because the size (5 nm) of MnO_2 nanoparticles simulated from the MnO_2 nanorods is smaller than that (40 nm) of Fe_3O_4 nanoparticles, tip effect promote MnO_2 nanoparticles to preferentially adhere to the MnO_2 nanoparticles on the surface of Fe_3O_4 nanoparticles. Due to the ferromagnetic nature of Fe_3O_4, the tip effect becomes weak with the length of rod-like nanostructure. For the formation of core-shell structured Fe_3O_4/MnO_2 nanocomposites (sample 3), the Mn/Fe ratio of 1:2 exceeded the reaction molar ratio in Eq.(4). The excessive $KMnO_4$ was decomposed slowly to MnO_2 under neutral or alkaline conditions (Eq.(5)).[23] Zhang et al reported that MnO_2 has a substantial number of hydroxyl radicals on the surface and a high affinity with Fe.[22] Therefore, the MnO_2 nanoparticles tended to deposit on the surface of the Fe_3O_4 nanoparticles forming the nanoshells.

$$FeSO_4+2NaOH\rightarrow Fe(OH)_2+Na_2SO_4 \quad (1)$$

$$3Fe(OH)_2+1/2O_2\rightarrow Fe(OH)_2+2FeOOH+H_2O \quad (2)$$

$$Fe(OH)_2+2FeOOH\rightarrow Fe_3O_4+2H_2O \quad (3)$$

$$9Fe(OH)_2+2KMnO_4\rightarrow 3Fe_3O_4+2MnO_2+2KOH+8H_2O \quad (4)$$

$$4KMnO_4+2H_2O\rightarrow 4MnO_2+3O_2+4KOH \quad (5)$$

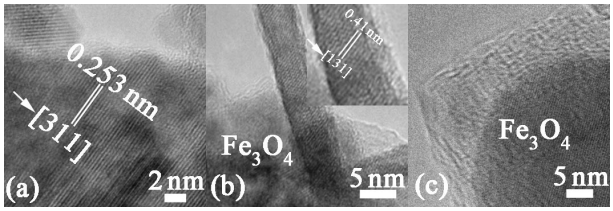

Fig.3 HRTEM images of (a) sample 1, (b) sample 2 and (c) sample 3. The inset of (b) is the typical HRTEM image of a nanorod in (b).

According to the transmit-line theory, the absorbing characteristics of the materials depend on a number of factors, including the frequency (f), sample thickness (d), relative complex permittivity ($\varepsilon_r=\varepsilon'-j\varepsilon''$) and relative complex permeability ($\mu_r=\mu'-j\mu''$). In order to investigate the effects on the EM wave absorption of three samples, the EM parameters of paraffin-bonded 40wt% three samples composites are measured at room temperature in the frequency range of 2-18 GHz, respectively. According to the Fig.5(a), both real (ε') and imaginary (ε'') parts of the ε_r of three samples-paraffin composites exhibit a similar tendency, i.e., declining significantly from 2 to 6 GHz and then decreasing slightly at higher frequencies. The phenomena can be ascribed to increased lagging behind of the dipole-polarization response with respect to the electric-field change at higher frequencies.[24] However, compared with those of the Fe_3O_4 nanoparticles-paraffin composite, both ε' and ε'' of the ε_r increase with the Mn/Fe ratio, which is similar with the Fe/MnO_2 composites.[25] According to the free electron theory, $\varepsilon''=\sigma/(2\pi f\varepsilon_0)$,[26] where σ is the electrical conductivity, the higher ε'' values of Fe_3O_4/MnO_2 nanocomposites at 2-18 GHz are indicative of higher electrical conductivities, attributed to the enhancement of MnO_2 nanostructures on the surface of Fe_3O_4 nanoparticles. MnO_2 itself is a kind of dielectric material with a permittivity as high as 16.[13] Therefore, by adding MnO_2, increased dielectric loss can be achieved in the Fe_3O_4/MnO_2 nanocomposites.

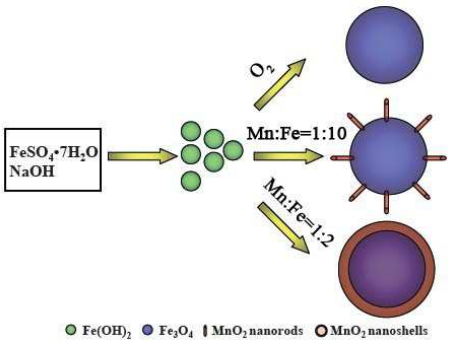

Fig.4 Schematic illustration of the formation procedure of the Fe_3O_4/MnO_2 nanocomposites.

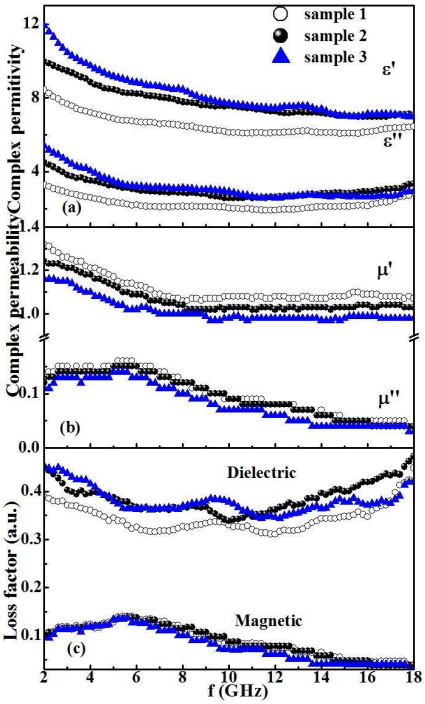

Fig.5 (a) Complex permittivity and (b) complex permeability and (c) dielectric loss factor and magnetic loss factore of three samples-paraffin composites.

The frequency dependences of the real part (μ') and the imaginary part (μ'') of μ_r of three samples-paraffin composites are shown in Fig.5(b). μ' curves display a similar tendency of decreasing with the frequency increasing from 2 to 18 GHz. In addition, the value of μ' reduces with the increase of Mn/Fe ratio. The decrease of μ' of the Fe_3O_4/MnO_2-paraffin composite can be explained by the introduction of paramagnetic MnO_2 component in the Fe_3O_4/MnO_2 nanocomposites. Compared with the variation of μ', there is no clear difference among the μ'' values of the different samples and the μ'' curves almost coincide. It can be found that a broad resonance peak around 3-6 GHz appears in the curves of μ'' and the resonance frequency remains almost unvaried with the ratio of Mn/Fe. As known, resonance frequencies depend strongly on the effective anisotropy field, which is associated with the magneto-crystalline anisotropy, on the magnetic-particle size and on the magnetic-particle geometry.[27, 28] For the as-prepared three samples, the Fe_3O_4 nanoparticles keep the similar size distribution and morphology, which can explain the reason why the resonance frequency remains almost unvaried.

The real parts and imaginary parts of EM parameters correspond to the energy storage and loss of EM waves in the propagation process, respectively. The dielectric loss factor (tan $\delta_E=\varepsilon''/\varepsilon'$) and magnetic loss factor (tan $\delta_M=\mu''/\mu'$) are commonly used to describe EM loss capacity, which can be affected by either the fillers in composites or the artificially periodic architectures.[1] As shown in Fig.5(c), the magnetic loss factor curves of three samples-paraffin composites are almost overlapped. On the other hand, the dielectric loss of Fe_3O_4/MnO_2-paraffin composites is larger than that of Fe_3O_4-paraffin composite over the whole 2-18 GHz. According to EM loss model, the Fe_3O_4/MnO_2 nanocomposites may exhibit the better microwave absorption performance than pure Fe_3O_4 nanoparticles in the whole frequency range of 2 to 18 GHz. From the dielectric loss curves of sample 2 and sample 3, we can get the following properties: (1) the dielectric loss of sample 3 is larger than that of sample 2 below 4 GHz; (2) the dielectric loss curves for two samples basically overlap in the frequency range of 4-9 GHz; (3) the dielectric loss of sample 3 is still larger than that of sample 2 in 9-11 GHz; (4) the dielectric loss of sample 2 exceeds that of sample 3 between 11 and 18 GHz.

The microwave absorption can be further quantitatively evaluated by the value of reflection loss (RL), in which -20 dB is equivalent to the 99% efficiency of microwave absorption. From the ε_r and the μ_r by using the Matlab procedure, the RL are calculated by using the formula of transmission lines,[2]

$$Z_{in} = Z_0(\mu_r/\varepsilon_r)^{1/2}\tanh[j(2\pi fd/c)(\mu_r\varepsilon_r)^{1/2}] \quad (1)$$

$$RL = 20\lg\left|(Z_{in}-Z_0)/(Z_{in}+Z_0)\right| \quad (2)$$

Where Z_0 is the impedance of free space, Z_{in} is the input impedance of the absorber, and c is the velocity of EM waves in free space.

The RL curves of the three composites with the thickness range of 1.5-5.0 mm can be calculated according to the Eqs (1) and (2), and the results are shown in Fig.6. The same characteristic of the three composites is that the RL peak moves to a lower frequency with the increase in thickness. However, the RL peak intensity and required peak frequency at the same thickness are different. Fig.6(a) shows that the RL values of sample 1-paraffin composite are smaller than those of composites including samples 2 and 3 at the same absorber thickness. For example, the optimal RL value of sample 1-paraffin composites with a thickness of 1.7 mm is -27.9 dB at 17.6 GHz, while the RL value of sample 2-paraffin composites is -41.5 dB at 16.8 GHz (Fig.6(b)) and that of sample 3-paraffin composites is -29.3 dB at 17.4 GHz(Fig.6(c)) for the same thickness. It is interesting that a RL peak (exceeding -25 dB) of three composites is located at 17-18 GHz due to the increase of dielectric loss factor at 17-18 GHz (Fig.5(c)). Compared with sample 1-paraffin composites, the absorption peaks of the samples 2-paraffin and sample 3-paraffin composites at the same thickness have shifted to a lower frequency, i.e., red shift. It is similar with the Ni/(C, silicides) nanocapsules, FeCo/C/$BaTiO_3$ nanocapsules and Ag-coated the Co_2Z barium ferrite composite, in which charge transfer at the interface gives rise to an electric dipole.[2, 30, 31] Fig.7 presents the difference of RL peak positions for sample 2-paraffin and sample 3-paraffin composites compared with sample 1-paraffin composites at the different thicknesses of the absorber. The red shift value of sample 2-paraffin composites is larger than that of sample 3-paraffin composites as the thickness increases from 1.7 to 2.5 mm and then the red shift values of paraffin-bonded composites with sample 2 and sample 3 are overlapped when the thickness is 3.0-5.0 mm.

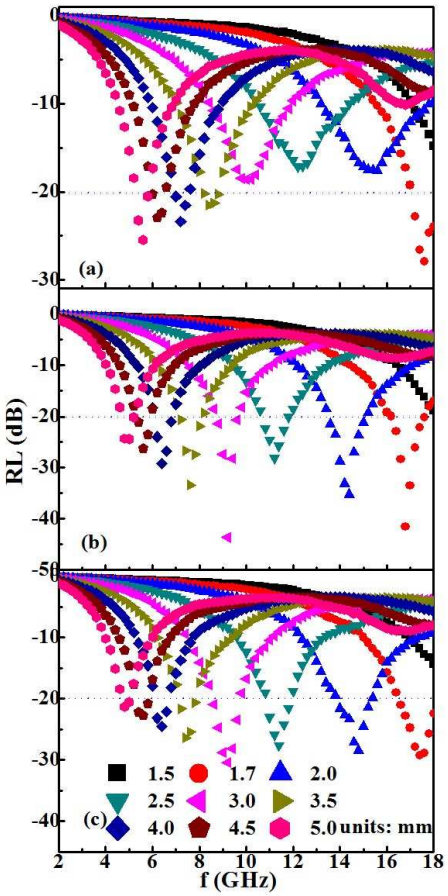

Fig.6 Calculated RL curves for (a) sample 1-paraffin, (b) sample 2-paraffin and (c) sample 3-paraffin composites.

When the EM wave penetrates into absorbents, the wave is absorbed through electron transitions. The MnO_2 nanostructures can cause the localization of electron density and generate additional energy levels near the Fermi level, which may reduce the electron transition energy.[30] Because of the reduction of the electron transition energy, the transition can occur at a lower frequency, which leads to the red shift of the absorption peak at different thickness of absorption layer. The difference between sample 2-paraffin and sample 3-paraffin composite is ascribed to the different geometrical morphology. The MnO_2 nanorods on the surface of Fe_3O_4 nanoparticles allow micronetwork to be formed.[31] The microcurrent can be produced in the frame of micronetwork, which can further reduce the electron transition energy.[32] Hence, the red shift value of sample 2-paraffin composite is larger than that of sample 3-paraffin composite when thickness is thinner than 3.0 mm. However, with the increase of thickness, the micronetwork will be destroyed by the paraffin and the sample preparation procedure. Hence, the red shift curves coincide when the thickness is thicker than 3.0 mm.

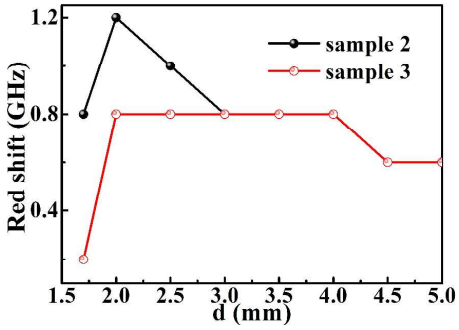

Fig.7. Compared with sample 1-parafin composite, the red shift of maximum RL peak positions for sample 2-paraffin and sample 3-paraffin composite.

As shown in Figs. 6(b) and 6(c), it is worthy noted that the RL peak values of the sample 2-paraffin and sample 3-paraffin composite both are obtained at the same frequency and the same thickness when the thickness is thicker than 3.0 mm. The phenomena may be ascribed to the overlapped dielectric loss and magnetic loss in the frequency range of 5-9 GHz. However, compared with the sample 2-paraffin composite, the sample 3-paraffin composite exhibits lower RL at different absorbent layer thickness as seen in Figs. 6(b) and (c), which cannot be explained reasonably by EM loss model. An optimal RL value (-43.6 dB) of sample 2-paraffin composite is larger than that (-30.5 dB) of sample 3-paraffin composite at 9.2 GHz with the thickness of 3.0 mm. For the magnetic/dielectric-loss absorbers, the excellent microwave absorption performance mainly results from proper EM impedance matching. In order to effectively estimate the EM impedance matching degree, a delta-function method has been proposed.[33] The delta-function can be described as,

$\Delta = \left|\sinh^2(Kfd) - M\right|$,where K and M are determined by ε_r and μ_r. The delta value should reach zero where RL approaches minus infinity. The smaller delta value represents better EM impedance matching. According to the delta-function using the measured ε_r and μ_r, the calculated delta value maps of the three samples-paraffin composites are shown in Fig.8. The blue area for Fe_3O_4/MnO_2-paraffin composites is obviously larger than that of Fe_3O_4-paraffin composites. The dark blue area (4.466) of Fe_3O_4/MnO_2 nanorods-paraffin composites slightly exceeds that (4.437) of Fe_3O_4/MnO_2 nanoshells-paraffin composites, which can explain the reason for the better microwave absorption ability of Fe_3O_4/MnO_2 nanorods. The RL and the delta values exhibit the same tendency, indicating that the enhanced microwave absorption performance of Fe_3O_4/MnO_2-paraffin composites would result from the good EM impedance matching through the special microstructure. Compared with the pure Fe_3O_4-paraffin composite, the remarkable enhancements on the microwave absorption performance of the Fe_3O_4/MnO_2-paraffin composite should be attributed to the improvements of ε_r and the dielectric loss factor and the proper EM matching induced by the special microstructure. Moreover, due to the MnO_2 nanorods on the surface of Fe_3O_4 nanoparticles, the produced microcurrent can reduce the electron transition energy, which contributes to the better microwave absorption in the Fe_3O_4/MnO_2 nanorods nanocomposites.

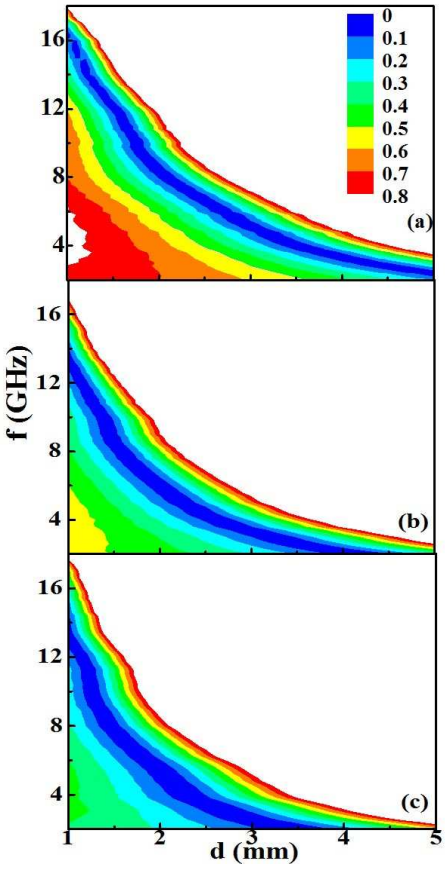

Fig.8. Calculated delta value maps of the paraffin-bonded composites with (a) sample 1, (b) sample 2 and (c) sample 3.

Conclusions

In summary, Fe_3O_4/MnO_2 nanocomposites have been synthesized by a simple and environmentally-friendly method. The morphologies of the prepared Fe_3O_4/MnO_2 nanocomposites were governed by adjustment of the molar ratio of Mn/Fe in the

precursor. When the molar ratio of Mn/Fe is 1:10, the prepared nanocomposites show the special microstructure, in which MnO_2 nanrods are formed on the surface of spherical Fe_3O_4 nanoparticles. With the increase of Mn/Fe ratio to 1:2, the core-shell structured nanocomposites with Fe_3O_4 nanoparticles as cores and MnO_2 as shells are obtained. The formation mechanism of Fe_3O_4/MnO_2 nanocomposites was proposed based on XRD, SEM and TEM results. Compared with the pure Fe_3O_4-paraffin composite, the remarkable enhancements on the microwave absorption performance of the Fe_3O_4/MnO_2-paraffin composite should be attributed to the improvements of ε_r and the dielectric loss factor and the proper EM matching. When the MnO_2 nanostructures are introduced into Fe_3O_4/MnO_2 nanocomposites, the absorption peaks of the Fe_3O_4/MnO_2-paraffin composites have a red shift compared with those of the Fe_3O_4-paraffin composites. The MnO_2 nanorods on the surface of Fe_3O_4 nanoparticles allow micronetwwork to be formed. The microcurrent can be produced in the frame of micronetwork, which can further reduce the electron transition energy. The special microstructure contributes to the better microwave absorption in the Fe_3O_4 nanoparticles/MnO_2 nanorods nanocomposites. As a result, Fe_3O_4/MnO_2 nanocomposites are attractive candidates for EM wave absorbers.

Acknowledgements

This study was supported by the National Natural Science Foundation of China (Grant No. 51201002).

Notes and references

[a]*School of Materials Science and Engineering, Anhui University of Technology, Maanshan,243002, China. Fax:+86 555 2311570; Tel: +86 555 2311570; E-mail: liuxianguohugh@gmail.com*
[b] *Center for Engineering practice and Innovation Education, Anhui University of Technology, Maanshan,243032, China.*
†Electronic Supplementary Information (ESI) available: See DOI: 10.1039/b000000x/

1 X.F. Zhang, P.F. Guan and J.J. Guo, Part. Part. Syst. Charact. 2013, 30, 842-846.
2 J.J. Jiang, D. Li, D.Y. Geng, J. An, J. He, W. Liu and Z.D. Zhang, Nanoscale 2014, 6, 3967-3971.
3 X.G. Liu, Q.Z. Ou, D.Y. Geng, Z. Han, Z.G. Xie and Z.D. Zhang, J. Phys. D: Appl. Phys. 2009,42, 155004
4. X.F. Zhang, J.J. Guo and G.W. Qin, Appl. Phys. Lett. 2014, 104, 252404.
5 D. Micheli, A. Vricella, R. Pastore and M. Marchetti, Carbon 2014, 77, 756-774.
6 A.B. Zhang, S.T. Liu, K.K. Yan, Y. Ye and X.G. Chen, RSC Adv. 2014, 4, 12565-13568.
7 H.M. Xiao and S.Y. Fu, CrystEngComm 2014, 16, 2097-2112.
8 S. Ryu, C.B. Mo, H. Lee and S.H. Hong, J. Nanosci. Nanotech. 2013,13, 7669-7674.
9 X.G. Liu, S.W. Or, S.L. Ho, C.C. Cheung, C.M. Leung, Z. Han, D.Y. Geng and Z.D. Zhang, J. Alloys Compd. 2011, 509, 9071-9075.
10 Y. Li, J. Zhang, Z.W. Liu, M.M. Liu, H.J. Lin and R.C. Che, J. Mater. Chem. C 2014,2, 5216-5222.
11 W.L. Song, M.S. Cao, Z.L. Hou, M.M. Lu, C.Y. Wang, J. Yuan and L.Z. Fan, Appl. Phys. A 2014, 116, 1779-1783.
12 M.H. Al-Saleh and U. Sundararaj, Carbon 2009, 47, 1738-1746.
13 H.T. Guan, J.B. Xie, G. Chen and Y.D. Wang, Mater. Chem. Phys. 2014, 143, 1061-1068.
14 S.F. Chin, S.C. Pang and M.A. Anderson, Mater. Lett. 2010, 64, 2670-2672.
15 X.L. Shi, M.S. Cao, X.Y. Fang, J. Yuan, Y.Q. Kang and W.L. Song, Appl. Phys. Lett. 2008,93,223112.
16 Y.P. Guan, J. Zhang, H. Jing and S.H. Liu, J. Solid State Chem. 2011, 184, 1165-1171.
17 M. Zhou, X. Zhang, L. Wang, J.M. Wei, L. Wang, K.W. Zhu and B.X. Feng, Mater. Chem. Phys. 2011, 130, 1191-1194.
18 M.Z. Xu, X.L. Shi, X.Q. Zou, H. Pan, M.D. Liu, K. Jia and X.B. Liu, J. Magn. Magn. Mater. 2014, 371, 20-28.
19 Y.P. Sun, F. Xiao, X.G. Liu, C. Feng and C.G. Jin, RSC Adv. 2013, 3, 22554-22559.
20 L.N. Wang, X.L. Jia, Y.F. Li, F. Yang, L.Q. Zhang, L.P. Liu, X. Ren and H.T. Yang, J. Mater. Chem. A 2014, 2, 14940-14946.
21 Y.P. Sun, X.G. Liu, C. Feng, J.C. Fan, Y.H. Lv, Y.R. Wang and C.T. Li, J. Alloys Compd. 2014, 586, 688-692.
22 Z.W. Zhao, J. Liu, F.Y. Gui, H.Feng and L.L. Zhang, J. Mater. Chem. 2012, 22, 9052-9057.
23 R. Deng, X. Xie, M. Vendrell, Y.T. Chang and X. Liu, J. Am. Chem. Soc. 2011, 133, 20168-20171.
24 H. Wang, H.H. Guo, Y.Y. Dai, D.Y. Geng, Z. Han, D. Li, T. Yang, S. Ma, W. Liu and Z.D. Zhang, Appl. Phys. Lett. 2012, 101, 083116.
25 W.Q. Zhang, S.W. Bie, H.C. Chen, Y. Lu, J.J. Jiang, J. Magn. Magn. Mater. 2014, 358-359, 1-4.
26 T. Draine and P.J. Flatau, J. Opt. Soc. Am. A Opt. Image Sci. Vis 1994, 11, 1491-1495.
27 F. Ma, Y. Qin and Y.Z. Li, Appl. Phys. Lett. 2010, 96, 202507.
28 H. Wang, Y.Y. Dai, W.J. Gong, D.Y. Geng, S. Ma, D. Li, W. Liu and Z.D. Zhang, Appl. Phys. Lett. 2013, 102, 223113.
29 J.J. Jiang, H. Wang, H.H. Guo, T. Yang, W.S. Tang, D. Li, S. Ma, D.Y. Geng, W. Liu and Z.D. Zhang, Nano. Res. Lett. 2012,7, 238.
30 Y.B. Zhang, F. Xu, G.G. Tan, J.L. Zhang, T. Wang and F.S. Li, J. Alloys Compd. 2014, 615, 749-753.
31 M.S. Cao, X.L. Shi, X.Y. Fang, H.B. Jin, Z.L. Hou and W. Zhou, Appl. Phys. Lett. 2007; 91: 203110.
32 P.C.P. Watts, W.K. Hsu, A. Barnes and B. Chambers, Adv. Mater. 2003, 15, 600-602.
33 Z. Ma, C.T. Cao, Q.F. Liu and J.B. Wang, Chin. Phys. Lett. 2012, 29, 038401.

